Heliyon 7 (2021) e06321

Contents lists available at ScienceDirect

Heliyon

journal homepage: www.cell.com/heliyon

Review article

Recent progress in surface plasmon resonance based sensors: A comprehensive review

Vasimalla Yesudasu [a], Himansu Shekhar Pradhan [a,*], Rahul Jasvanthbhai Pandya [b]

[a] Department of ECE, National Institute of Technology Warangal, 506004, TS, India
[b] Department of EE, Indian Institute of Technology Dharwad, Karnataka, 580011, India

ARTICLE INFO

Keywords:
Detection accuracy
Fiber based-surface plasmon resonance
Figure of merit
Sensitivity
Surface plasmon resonance
Quality factor

ABSTRACT

In the recent years, researchers have contributed substantially in the field of Surface Plasmon Resonance (SPR) sensors and its applications. SPR sensors show the salient features, such as label-free detection, real-time monitoring, small sample size, furnish accurate outcomes at low cost, and smooth handling. Moreover, the SPR sensors are also well-known because of its quantitative and qualitative excellent performance in real-time applications, including drug discovery, environment monitoring, food safety, medical diagnosis, clinical diagnosis, biological studies, and biomolecule interactions. This paper exhibits a comprehensive review of SPR based sensors, such as prism-based SPR with the applications (e.g., biomolecule interaction, medical diagnostic, etc.), fiber-based SPR, and waveguide-based SPR. Furthermore, we summarized the modern designs and techniques with their limitations and challenges in detail. The erudition outlined in this paper can be given an exceptional benefit for the researchers and industry people in the field of SPR based sensors.

1. Introduction

Surface Plasmon Resonance (SPR) is an efficient mechanism to retrieve the erudition of optical properties, such as nanomaterial and biomaterial. The resonant oscillation of the conduction electrons are formed at the interface of negative-positive permittivity content due to the incident p-polarized light. SPR sensor depends on several tools for assessing the absorption of various materials on the metal film (gold (Au), silver (Ag)). It begets multiple applications, such as food safety, drug discovery, environment protection, and medical diagnostics. Therefore, many researchers have been focusing on improving the sensitivity (S) of the SPR sensors employing novel sensor structures. The first employment of the SPR procedure as a sensor was published in [1]. In the early 20th century, R. W. Wood had perceived the p-polarized light incident on the surface of the diffraction grating, and observed the pattern of irregular light and dark lines that occurred in reflected light [2]. In 1907, J. Zenneck et al. was introduced the solution of the surface wave (SW) to Maxwell's equations. Electromagnetic waves (EMW) prevail at the periphery of two mediums of the lossy and loss-free medium due to plasmons' oscillation. Moreover, the lossy (imaginary) dielectric function is incumbent for binding the EM wave and interface [3]. A. Sommerfeld noticed that J. Zenneck's hypothesized magnitudes fields of SWs diverse inversely proportional to the square root of the distance from the dipole source [4]. In addition, it is a high-speed wave and exponentially decomposed with height above the boundary. In 1957, a significant development was accomplished toward the SPR hypothesis, when R. H. Ritchie theoretically confirmed the presence of metal surface plasma excitations (SPE) [5]. C. H. Powell et al. determined that those surface plasmons (SPs) were excited by employing electrons at metal interfaces [6]. Later, E. A. Stern et al. observed that EM waves on a metal surface contained EM radiation combined with plasmons. They also extracted the dispersion relationships on metal surfaces for SPWs [7]. In 1968, A. Otto fabricated the Attenuated Total Reflection (ATR) prism coupled method to permit the coupling of large EM light waves with EM-SWs [8]. Single crystal surface analyzed by employing the Otto configuration. This configuration acquires some gap between the prism and metal surface, and result of that no more metal surface is affected by the prism. Similarly, the Kretschmann configuration is also the conventional configuration, which had inverted by E. Kretschmann. It utilizes a 10–100 nm thickness of metal coated on the prism surface, and SPs have subsisted on that surface [9]. X.D. Hoa et al and J. Homola et al. presented a significant review on the SPR sensor technology [10, 11], summarizing the essential areas of applications, different techniques (e.g., interferometry and luminescence) [12] used to analyze the

* Corresponding author.
E-mail address: hsp@nitw.ac.in (H.S. Pradhan).

https://doi.org/10.1016/j.heliyon.2021.e06321
Received 15 November 2020; Received in revised form 21 January 2021; Accepted 16 February 2021

performance of chemical and biological sensors. A brief description of the physical and chemical/morphological characteristics are essential for the optical sensors, which were incorporated inclusive of the sensor's operating theory. Another research stressed the condition of various chemical sensors and biosensors for fiber optics [13]. A. K. Sharma et al. also presented a comprehensive review on the fiber-based sensors [14]. Considering the aforementioned state of the art, the detailed review of the SPR-based sensors remains absent. Hence, this article summarizes SPR-based sensors such as prism-based, fiber-based, and waveguide-based SPRs for various applications, such as environmental protection and bio-molecular interaction. The article has been arranged as follows: sections- 2 demonstrated the principles, methods, evaluation of the prism-based SPR sensor; section-3 and 4 described the fiber-based SPR and waveguide-based SPR sensor, respectively. Section-5 exhibits its future scope and finally, ended with a conclusion of the presentation.

2. Surface Plasmon Resonance (SPR) sensor

2.1. Plasmon oscillation

Chemistry proposed the delocalized electrons that are dissociate to a covalent bond and incoherence. Metal signifies an excellent conducting material and a regular array of atoms. An atom preserves at least one electron and free to impel around and distributed amidst all other particles in the material. These free electrons can generate an infinitely large mass that are distinct from positive ions. Consequently, the Jellium model demonstrated that a constant positive charge background could replace these ions. Nonetheless, the whole charge density settles at zero within the conductor. A peripheral field applies on the conductor, and it transpires the free electron oscillation that degraded the free electrons' mass. In that case, the negative free electrons are no longer veiled by the background, and they begin to get attracted by the positive ion. The covalent of these electrons and positive ions occurred in the background, and it unfolds with a density higher than necessary to acquire charge neutrality. At the Coulomb repulsion, a restoring force generates and executes the longitudinal oscillations among the free electrons, known as plasma oscillations. Quantum of the plasma oscillation is a plasmon, and the subsistence of plasma oscillations was describing in an electron energy loss experiment [15, 16].

2.2. Surface plasmon oscillation

The classic drude conductive model describes some metal's characteristics, but not all of them are successful. The discovery of Bose-Einstein statistics and the development of quantum mechanics explains the rest of the story. Light implies an EM wave, and when it strikes the metal as described in Figure (1a), then the electric field of light interacts with conducting electrons in the metal. Atoms indicate that the quantum members are apprehended as fermions, and the oscillation of these electrons can transpire a wave pattern spatial distribution of the particles. This wave pattern is termed a surface plasmon wave (SPW) or surface plasmon polaritons (SPPs). After transpiring the SPW, it opposes the light energy, which is bearing in plasmons, as in Fig. (1b); The light absorbs its energy and converts it into a reflected light is a working principle of the SPR sensors.

Moreover, plasmon oscillation transpired at the M-D interface. The charge density of these oscillations with the M-D interface is identified as surface plasmon oscillation, and the quantum of these oscillations is known as a surface plasmon. These SPs are escorted by a longitudinal P-polarized electric field, decaying exponentially in metal and dielectric, as shown in Figure 2. The consequence is that the field produces maximum intensity at the metal-dielectric (M-D) interface. These asserts achieve by unlocking Maxwell's numerical equation for the M-D category of refractive index (RI) allocation. The SPW propagation constant (PC) (K_{sp}) is endless within the M-D interface, and mathematically mentioned in an Eq. (1).

$$K_{sp} = \frac{\omega}{c}\sqrt{\frac{\varepsilon_d \varepsilon_m}{\varepsilon_d + \varepsilon_m}} \tag{1}$$

Here ω is the incident frequency, c is the velocity of light, ε_d and ε_m are the dielectric constant of the dielectric medium and the metal film, respectively. $\varepsilon_m < 0$ signifies the metal, and $\varepsilon_d > 0$ signifies the dielectric medium at a given wavelength. Eq. (2) represents the more significant PC of the light wave at the propagation frequency via the dielectric medium. Figure 3 represented the distribution curves (K_{sp}), and the direct light incident through the dielectric medium (K_s). The SPs' PC is higher than the light wave in the dielectric medium, and the consequence that non-radiative SPs excited at the M-D interface, i.e., direct light cannot excite the SPs. Therefore, the wave vector of exciting light in the dielectric medium must be increase for SPs excitation.

$$K_s = \frac{\omega}{c}\sqrt{\varepsilon_d} \tag{2}$$

2.3. Types of configurations

The reflected photons in total internal reflectance (TIR) procreate an electrical field on the interface's opposite site. The plasmons develop a comparable area on either side of the metal film that spread out into the dielectric medium. This wave designated as evanescent wave (EW) because the wave magnitude decreases exponentially with sprouting distance from the surface of the interface, decaying over a range of one light wavelength. Figure 4 represented the Otto configuration operates with an ATR principle, which transpired at the prism base coupling. An incident light applies at an angle higher than the critical angle at the prism-air (P-A) interface for the coupling of SPW with EW [17]. EW decays exponentially in the dielectric medium adjacent to the metal layer since both waves own the PC along with the interface. Therefore, a strong

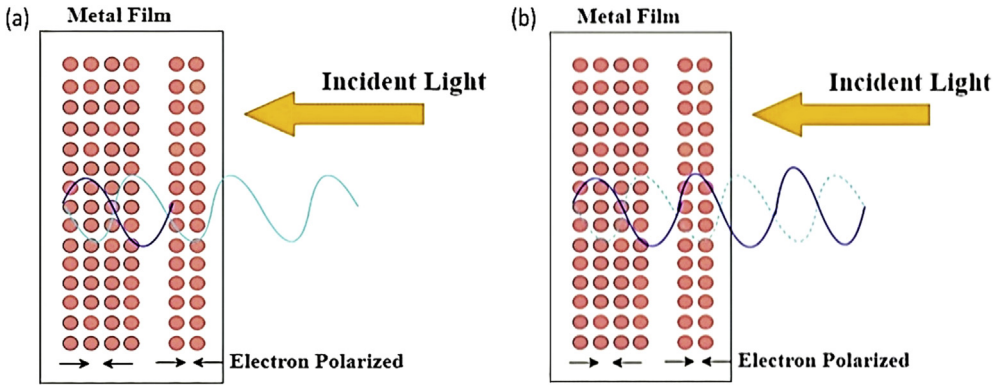

Figure 1. (a) Phenomenon of metals (b) Reminiscent of Lenz's law.

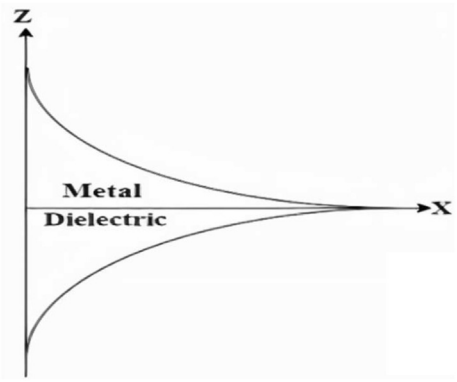

Figure 2. Exponential intensity field for surface plasmon (SP) in metal and dielectric (M-D) layers (X-axis signifies the metal-dielectric interface and Z-axis illustrates the field intensity).

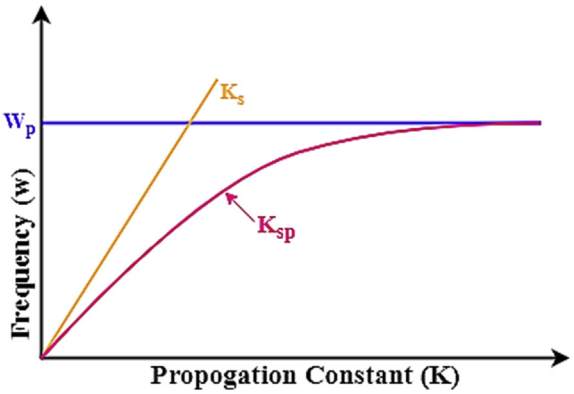

Figure 3. Distribution curves for surface plasmon wave (K_{sp}), and the direct light incident through the dielectric medium(K_s).

possibility of interface developed amid these waves. Eq. (3) denotes the x-component of the wave PC of the EW at the P-A boundary.

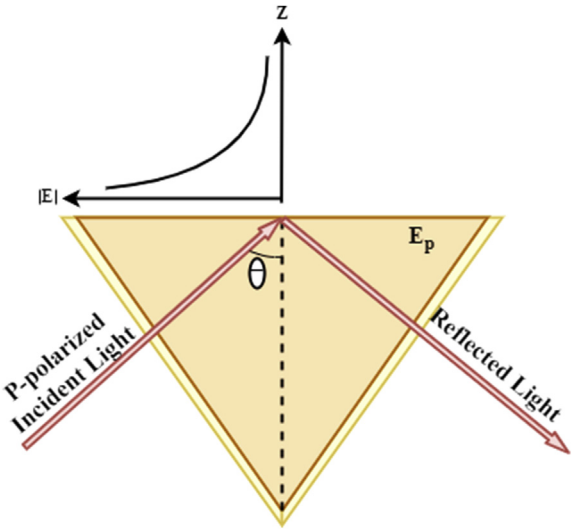

Figure 4. Design of excitation of evanescent wave (EW) on the metal-dielectric (M-D) interface.

$$K_{ev} = \frac{\omega}{c}\sqrt{\varepsilon_p}\sin\theta \tag{3}$$

Furthermore, Figure (5a) represents the Otto configuration that exposed a gap flanked by the prism and metal film. Exponential decay of the evanescent field at the P-A interface and this field can excite the SPs at the air-metal (A-M) boundary. Moreover, the configuration is rigid for the practical realization, but it's beneficial in analyzing the single-crystal metal surfaces and adsorption. Fig. (5b) represents the Kretschmann configuration, where a metal film is coated on the prism instead of air. An evanescent field spawned at the prism-metal (P-M) interface, diminishing the attenuation due to the environmental effects. This field can excite the SPs at the metal-air (M-A) interface. Figure 6 concludes that the PC of the EW could match with that of the SPW at the M-D interface relying on the frequency and incidence angle. Moreover, no excitation of SPs at the M-P interface, because of the PC of SPW lies to the maximum of EW's PC. Eq. (4) denotes the resonance condition, where minimum reflectance (R_{min}) transpired for the response of SPR phenomenon [14].

$$\frac{\omega}{c}\sqrt{\varepsilon_p}\sin\theta = \frac{\omega}{c}\sqrt{\frac{\varepsilon_d\varepsilon_m}{\varepsilon_d+\varepsilon_m}} \tag{4}$$

Where ε_p is the dielectric constant of the prism, θ_{res} is the resonance angle. Figure 7 represents the θ_{res}, is defined as the angle at with reflectance is minimal, and it varies according to the device parameters, such as the wavelength of light and RI of material. Figure 8 represents the θ_{res} fluctuation as a function of the RI. The fundamental performance parameters, such as S, detection accuracy (D.A.), and quality factor (Q.F.) should be as high as possible for the beneficial sensor, and as well as numerical measurements inspected from Eqs. (5), (6), and (7), respectively. Moreover, higher S represents the sensor's immediate response capability, detecting the minor change in the RI. High D.A. serves the SPR sensor's ability to contribute to accurate outcomes, where high Q.F. represents the sensor's quality. $\nabla\theta_{res}$represents the change in the resonance angle shift, and the full-width-half-maximum (FWHM) defined the full width at half of the maximum reflectance of the sensor. Eq. (5) testifies the S is proportional to the resonance angle change, and Eqs. (6), (7), and (8) testifies the D.A., Q.F., and figure of merit (FOM) are inversely proportional to the FWHM.

$$Sensitivit\ y\ (S) = \frac{Change\ in\ resonance\ angle\ (\theta_{res})}{Change\ in\ refractive\ index\ (\nabla n)} \tag{5}$$

$$Detection\ Accuracy\ (D.A.) = \frac{Change\ in\ resonance\ angle\ (\theta_{res})}{Full\ width\ half\ \text{maxima}\ (FWHM)} \tag{6}$$

$$Quality\ Factor\ (Q.F.) = \frac{Sensitivit\ y\ (S)}{Full\ width\ half\ \text{maxima}\ (FWHM)} \tag{7}$$

$$Figure\ of\ Merit\ (FOM) = S \times \frac{(1 - \text{minimmum Reflec tan ce}\ (R_{\min}))}{Full\ width\ half\ \text{maxima}\ (FWHM)} \tag{8}$$

2.4. Evaluation of prism-based sensor

Figure 9 shows the prism-based SPR sensor that is coated with metal film (i.e., Au, Ag, aluminum (Al), copper (Cu)). The achievement of the SPR sensor was enhanced by employing metamaterials on the metal surface. The numerical analysis of SPR response with metamaterial furnished better performance than the conventional SPR sensor in visible range wavelength. Y. K. Prajapathi et al. had compared the results with standard four and five-layered SPR sensors. The metamaterial contributed a broader dynamic range or efficient range of computable RI rises. The metamaterial acquires several advantages for increasing the resonance dip of optical SPR sensor, that leads to higher S of the sensing resolution and dynamic range [18,19]. J. B. Maurya proposed two different SPR sensors for performance improvement by employing various types of prisms (BK7, SF11, and 2S2G), and metal materials (Au,

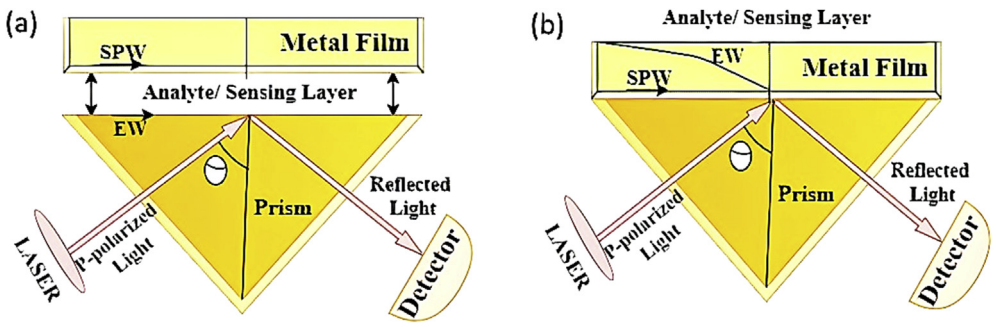

Figure 5. SPR configurations: (a) Otto configuration (b) Kretschmann configuration.

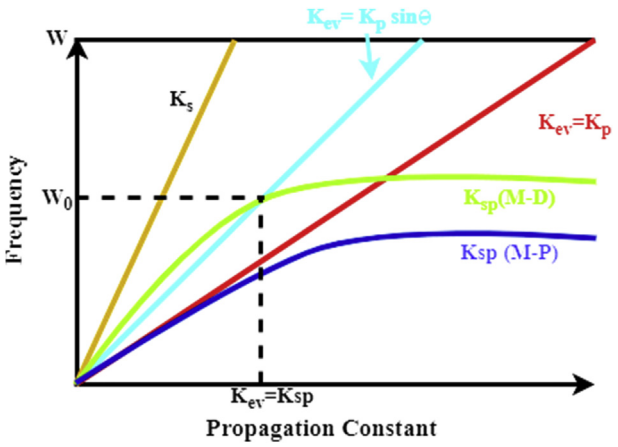

Figure 6. Dispersal curves for EW-K_{ev}, K_s, K_{sp} at the metal-dielectric (M-D), and the metal-prism (M-P) interface.

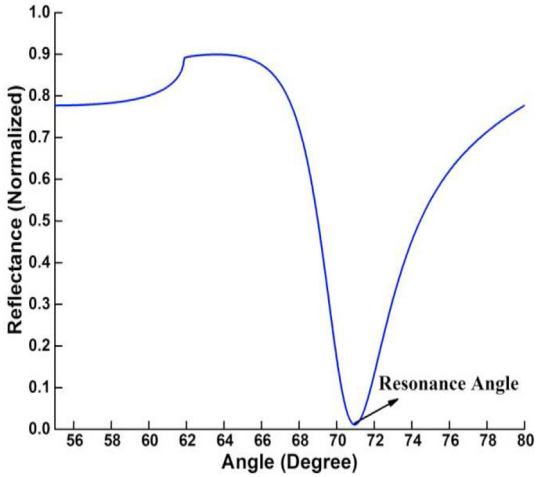

Figure 7. SPR response in terms of reflectance by applying angular interrogation and sharp dip of the curve is a resonance angle (θ_{res}).

Ag, Cu, and Al) at 632.8 nm wavelength. Initially, the authors optimized each metal film's thickness and then elected the most desirable SPR performance content by comparing S, FWHM, and R_{min} parameters. Eventually, the authors concluded the Ag renders high-Q.F., resolution, and Cu contributed immeasurable S [20]. S. Pal et al. introduced the new 2D material i.e., black phosphorus (BP)-based SPR for enhancing the performance parameters were estimated at 633 nm wavelength. The BP furnished the S of 1.42 and 1.40 times greater than the conventional SPR and the graphene-based SPR, respectively. This vast performance furnishes from the unique optical properties, such as bandgap, higher charge mobility, and increased binding of molecules on the surface sensor, but it renders little D.A [21]. M. S. Rahman et al. incorporated the MoS_2 monolayer between the standard graphene and Au for enhancing the S. The sensor S of 89.29°/RIU and 87.8°/RIU for double and monolayer of the graphene-MoS_2 hybridization layers, respectively. The proposed SPR with monolayer MoS_2 has furnished the S of 10% higher than the without MoS_2 [22]. The MoS_2 proffers more agreeable Q.F. and R_{min} performance than the graphene with a minor diminished amount of D.A. and S [23, 24]. Furthermore, J. B. Maurya had utilized the dielectric material for grater enhancement of the SPR sensor performance. The numerical analysis of the SPR is evaluated at 632.8 nm wavelength and concluded that all performance parameters alter according to the sensing region's RI. The RI real part is directly proportional to the half-width half maxima (HMHM) and inversely comparable to the R_{min}. The RI imaginary part dielectric material is inversely proportional to the HMHM and directly proportional to the R_{min} [25]. The Silicon (Si)'s influence in SPR performance improvement employing a hybrid MoS_2-Graphene structure was demonstrated in [23]. The MoS_2 layers were proportional to the S of the sensor at uniform graphene thickness. Moreover, Si affords massive D.A. and Q.F. but degrades the little amount of S [26]. The numerical analysis of SPR sensor was performed at infrared wavelength, i.e., 1000nm, employing metamaterials. The metamaterial RI and thickness of ($n_{mat} = -\sqrt{\varepsilon_{mat}\mu_{mat}}\ \mu_{mat}$= -2.4 + 0.001i, ε_{mat}= -4 + 0.001i), 349 nm, respectively. The RI of binding (ssDNA) layer n_b= 1.462, 1.466, 1.468. Finally, the sensing medium RI of before and after adsorption of bimolecular are 1.33 and 1.35, respectively. The metamaterial enables massive S of more than 300°/RIU. The S varied from 326.56°/RIU to 454.36°/RIU at n_b = 1.46; 327.19°/RIU to 468.11°/RIU at n_b = 1.466; and 341.16°/RIU to 489.88°/RIU at n_b = 1.468 [27]. The S improvement with decayed D.A. and Q.F. has been presented in [28]. The SPs transpired at THz frequency for one of the prominent applications, such as biomedical sensing. The sensor affords the S of 147°/RIU for varying the different RI of gas sensing medium. Y. Xiang et al. exhibited these plasmonic waves that own the same properties as plasmonic waves in optical range wave by virtue of SPW's constraints within the boundary at THz frequency [29]. The angle and wavelength interrogation of the Al-based SPR sensor performance was performed theoretically and experimentally with the trapezoidal BK7 prism. The Al performance was compared with other metal film material, such as Ag, Au, and Cu. The Al improved in de-ionized water by Al-surface oxide and constrained significant sensor degradation [30]. The performance analysis of graphene-based SPR was proposed with a 13% improvement of S compared with existing work at 632.8 nm, where metal film thickness remains constant. The RI (thickness) of the prism SF10, Ag, MoS_2, Graphene, single-standard Deoxyribonycic acid (ssDNA), and water are 1.7786, 0.005625 + 4.276i (37 nm), 5.9 + 0.8i (M × 0.65 nm), 3 + 1.149106i (G × 0.34 nm), 1.462 (3.2 nm) and 1.3317, respectively [31]. The summary of the performance enhancement of the SPR sensor with some configurations has been presented in Table 1. The maximum S of 237.5°/RIU performance furnishes

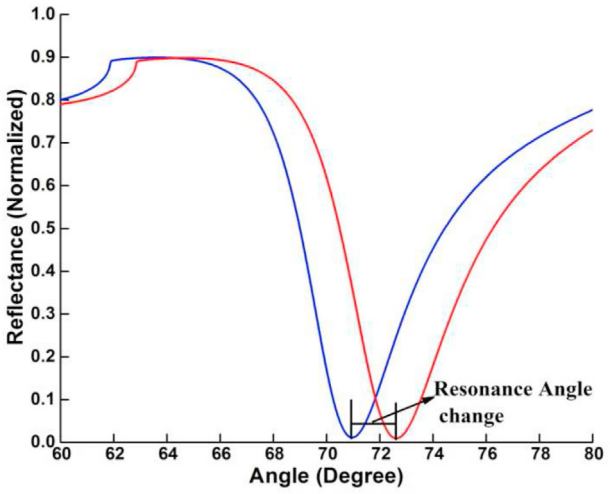

Figure 8. The resonance shift ($\nabla\theta_{res}$) with respect to the RI change (∇n). (Blue curve represents the SPR curve at sensing RI (n_s), and red curverepresents SPR curve after sensing RI change (∇n_s)).

with monolayer tungsten diselenide (WSe_2) and seven layers of Si thickness [32]. The S subsists non-linear with the number of graphene layers and the SPR frequency, i.e., surface resonance frequency (SRF), whereas linear in the existing work. The SRF and SPW's propagation velocity are calculated by employing Eqs. (9) and (10).

$$SRF = \frac{c_0}{n_{geo}} \frac{K_{SPW}}{2\pi} \tag{9}$$

Where,

$$K_{SPW} = \frac{2\pi}{\lambda} n_p \sin\theta_{SPR} \tag{10}$$

$\frac{c_0}{n_{geo}}$is the propagation velocity of SPW which is perpendicular to the confined evanescent EM wave, n_{geo} is $\sqrt[3]{n_{Au} n_S n_G}$. Where n_{Au} represents the gold's RI, n_S represents the RI of sensing medium, and n_G represents graphene RI [33]. The Otto configuration SPR structure was designed with various combinations of the nano-composite and metal materials for the enrichment of S. The sensor results demonstrated the enormous S of 200°/RIU at six layers MoS_2 and monolayer graphene with TiO_2–Au composite material at 30 nm thickness [34]. M.S. Islam et al. had presented the study of excitation, nature of SPs, EM field distributions, and magnitudes at both conventional and multilayer SPR structures. The SPWs transpired when the polarized light flows parallel to the interface. The strong plasmon-induced on the sensing interface and capture less reflected light at resonance condition and vice-versa [35]. S. Pal was designed the BP-based SPR sensor with the consolidation of Au, Si, and Transition Metal Dichalcogenides (TMDC) materials, such as WS_2 and WSe_2 for the enrichment of sensor S. The performance shown in terms of S, R_{min}, and FWHM. The sensor accomplished preeminent S of 184.6°/RIU with TMDC material and 163.1°/RIU without WS_2 [36]. R. Boruah el at. have designed the novel Kretschmann SPR setup with double prisms for the performance improvement of the sensor. This structure affords numerous advantages, such as intense output signals, wide-angular scan-ranges. The high RI of prism yields different sensors, such as gas sensors and fluid biosensors, to operate with a wide dynamic range [37]. A. A. Michelson et al. inverted the interferometer and rotator, which accomplishes the phase and angle interrogation. The sensor was designed experimentally with the S of 7.2×10^{-7} RIU/0.1°, and FOM of 316 at 1 to 1.4 range [38].

S. K. Raghuwanshi et al. was designed a novel SPR sensor by employing Teflon and metamaterial surfaces for powerful bio-recognition to explore the multi-layer sensor structure's dispersion-customized properties. The author employed this sensor to improve the S because it deducts side lobes' virtue in a dual-mode, diminishing the S. Moreover, the importance of SPW excitation methods for the sensors' design was also revealed in [39]. C. A. De Souza Filho et al. described the effects of the SPR biosensor, such as documented disturbances, noise, the incident light's temperature, and wavelength. In additional, this design permits each component and the entire system to be evaluated individually. A solution had presented to achieve increased energy-efficiency and facilitates handheld mobile phone-based sensors [40]. S. Scarano, et al. and M. Faca et al. were exhibited the analytical instruments as profitable and flexible diagnostic tools for an assortment of applications in bioanalytical chemistry, such as SPR and SPR imaging. The bio-receptor was immobilized on the bio-chip to decide the above systems' selectivity and ranges from the nucleic acid sequence to proteins, antibodies, and new synthetic bio-receptors. It enables label-free and multi-analyte detection. Moreover, a wide range of molecular weight target analytes can adapt to multiple assay designs, ranging from small molecules to living cells [41,42].

2.5. SPR biosensor applications

The biosensor technology has been enriching to prevail the bind enlightenment of the DNA molecular diagnosing over and above 400 diseases, and this enumeration increases further. SPR sensors unfold

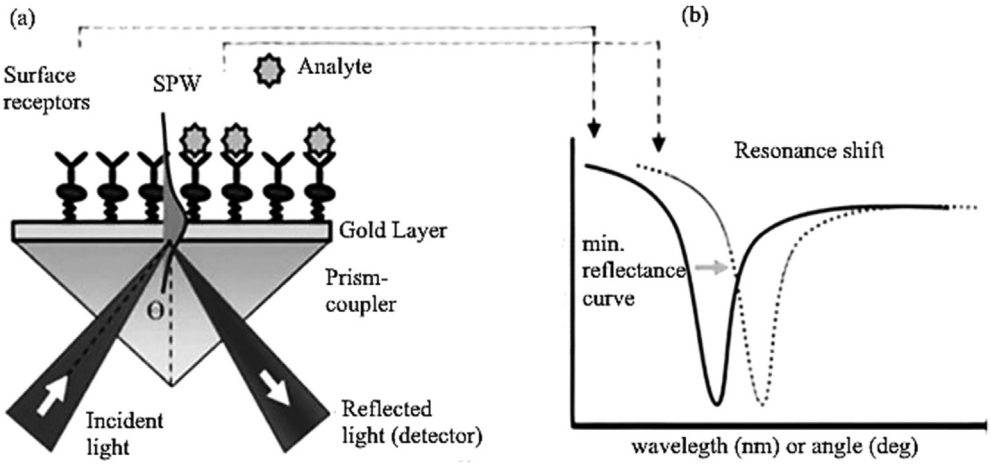

Figure 9. (a) Canonical structure of the Prism-based SPR sensor employing Kretchsmann configuration (b) Resonance/wavelength Shift in reflectance curve according to the RI changes in a medium [10, Figure 1].

Table 1. Summary of the state of the art in Performance Enhancement of the SPR Sensor at 633 nm Wavelength.

References	Configuration	Performance Parameters			Conclusion
		S (°/RIU)	D.A.	Q.F. (RIU^{-1})	
Y. K. Prajapathi et al. 2013 [19]	Prism + Ag + Metamaterial + Ag + Au + Water	-	-	-	The SPR sensor has the advantage of improving reflectance dip and S by employing the metamaterial layer.
J. B.Muryaet al.2015 [24]	Prism + Au + MoS_2 + Affinity + Water	48.82	0.615	5.12	The SPR sensor proposed the effect of Si between metal and MoS_2.
	Prism + Au + Si + MoS_2 + Affinity + Water	48.65	10243	85365	
J. B.Murya et al.2016 [23]	Prism + Si + Graphene + Affinity + Sensing Layer	49.86	14.54	207.75	The sensor Ag + Graphene/MoS_2) presents the acceptable S, but the D.A. and Q.F. are substantially higher than the existing work.
	Prism + Si + MoS_2+ Affinity + Sensing Layer	49.29	17.25	246.45	
J. B.Murya et al.2017 [25]	Prism + Metal + Dielectric + Water	-	-	-	The purely real part RI of the dielectric layer offers the contradicted results between $\nabla\theta$ and HWHM. To mitigate this problem increase the imaginary part of the complex RI of dielectric medium.
J. B.Muryaet al.2016 [20]	Prism BK7/SF11/2S2G)+ Metal Au/Ag/Cu/Al)+ MoS_2+Graphene + Water	-	-	-	Ag furnishes the lower FWHM, which leads to high D.A. and Q.F.; Cu renders high $\nabla\theta_{res}$, which leads to higher S.
J. B.Muryaet al. 2018 [54]	Prism + AuNPs + MoS_2+ Affinity + Water	107.29	0.50	7.16	The monolayer and bilayer MoS_2 furnish the highest S than the graphene-based sensor.
M. S.Rahmanet al.2017 [22]	Prism + Au + MoS_2+ PBS solution	89.29	0.919	13.13	The hybrid structure of MoS_2-Grpahene is appropriated to enhance the S of the SPR sensor.
S. Palet al.2017 [21]	Prism + Au + BP + Affinity + Sensing Layer	180	0.29	-	The BP and BP-Si based structures render the highest S and D.A., respectively. These are almost constant with a variation of sensing RI.
	Prism + Au + Si + BP + Affinity + Sensing Layer	115	1.19	-	

several sensing applications for biochemical materials because the reduced pre-processing and can also be measured in real-time. Few authors were established the SPR sensor to detect DNA hybridization at visible range wavelength. Two desirable parameters are required for the adequate SPR sensor performance, such as high S and FOM. The concentration between of RI before and after hybridization and the shift in the concentration of phosphate-buffered saline (PBS) solution has been linked by the subsequent expression presented in Eq. (11).

$$n_H = n_S + c_a \frac{dn}{dc} \tag{11}$$

Where, n_H is the sensing medium RI after hybridization, n_S is the sensing medium RI before hybridization, c_a is the concentration of an adsorbed molecule, and dn/dc is the increment in RI due to the adsorbed molecule. After its realization through current manufacturing technology, the suggested sensor can effectively diagnose complicated diseases, such as cancer and hepatitis B on DNA hybridization. M. S. Rahman et al. proposed the BP-based SPR sensor to detect the DNA with S of 125°/RIU and Q.F. of 13.62 RIU^{-1} [43]. He demonstrated the WS_2 based SPR sensor achieving the high resolution than the graphene-based SPR sensor for DNA detection. This SPR sensor owns the capability of distinguishing between complementary and single based mismatched DNA with S of 95.71°/RIU at the optimal gold film [44]. Two-dimensional (2-D) and TDMC materials persist attractive for the enrichment of the SPR sensor performance in terms of S for DNA hybridization. S. Ahmed et al. suggested the WS_2-BP-based SPR sensor with a maximum S of 187°/RIU subsists of 10 layers of BP, and WS_2 monolayer. The high performance of sensors can possess prospective applications in medical diagnosis and detection of biochemical [45]. A novel SPR structure was proposed in [46] employing Ag, Si, and BP to enhance the performance parameters, such as S, D.A., Q.F. and FOM. The sensor furnished the highest S of 91.54°/RIU for the Ag-BP based sensor; D.A. of 69, Q.F. of 1061.6 RIU^{-1}, and FOM of 554.58 for the Ag-Si-BP based sensor. The review of the state of the art on SPR sensors for DNA hybridization has been presented in Table 2.

Furthermore, biomarkers for protein inadequacy can be detected in body fluids, such as saliva, urine, and blood plasma [47]. W. Wu et al. was exhibited the protein detection performance at concentrations ranging between pg/mL to g/mL. For an instant, the levels of the human chorionic gonadotropin and the activated leukocyte cell adhesion molecule in the blood plasma of healthy individuals sojourn approximately 1 ng/mL [48] and 100 ng/mL [47], respectively. The numerical analysis of the germanium (Ge)-based SPR sensor has been presented with a maximum S of 132°/RIU at the thickness of 1.5 nm where the RI of protein, i.e., Bovine serum albumin 1.435. Ge-graphene-based affords an

Table 2. Review of the state of the art on SPR Sensor for DNA Hybridization at 633 nm Wavelength.

References	Configuration	Performance Parameters				Conclusion
		S (°/RIU)	D.A.	Q.F. (RIU^{-1})	FOM	
M. S. Rahman et al. 2018 [43]	Prism + Au + WS_2+ Graphene + Sensing Layer.	95.71	1.763	25.19	-	The sensor is capable of differentiating between the complementary and single-base mismatched DNA.
S. Pal et al.2018 [44]	Prism + Au + BP + Graphene + Sensing Layer	125	0.95	13.62	-	The sensor can work efficiently to detect the hybridization of DNA.
B. Meshgi-nqalamet al.2018 [45]	Prism + Chromium + Au + BP + TDMC Material + Sensing Layer	187.22	0.10	-	18.72	Ten layers of SPR Structure BP/monolayer WS_2 provides aimprovedS and FOM.
Y. Vasimalla et al. 2020 [46]	Prism + Ag + BP + Graphene + Sensing Layer	91.54	3.61	54.81	54.78	The sensor can efficiently detect the DNA hybridization with high-performance parameters such as S, D.A., Q.F., and FOM.
	Prism + Ag + Si + BP + Graphene + Affinity + Sensing Layer	53.08	69	1061.6	554.58	

S of 16% more than the only graphene-based SPR biosensor. Therefore, the authors concluded the Ge exhibited a better option for detecting protein detection by SPR biosensor [48].

The kidneys play a crucial role in sustaining human health, signifying environmentally beneficial, and surviving a highly complex waste disposal arrangement. They are proficient in a continuous sorting method of non-recyclable scrap from recyclable scrap and cleans the blood via filtering blood to exclude toxins and wastes. The novel Cu-Gr-based SPR structure design with BSG prism for urea detection at near-infrared range wavelength. The FWHM transpires directly proportional to the Cu thickness at uniform urea RI of 1.49 [49]. The numerical analysis performance of the SPR sensor performed at 670 nm and 785 nm wavelength. Urea RI fluctuates from 1.335 to 1.347, such as 1.335, 1.337, 1.339, 1.342, and 1.347 with concentration fluctuate at the concentration of 0.625 ml/dl, 1.25 ml/dl, 2.5 ml/dl, 5 ml/dl, and 10 ml/dl, respectively [50]. The aluminum oxide-based sensor was proposed in [52], which demonstrates the 3.58% and 5.24% improvement in S at the RI of 1.33433 and the concentration of 50nM [51].

Waterborne disease-related bacteria is the world's most significant health predicament. The advancement of new technology to deliver sustained drinking water yields tremendous effort into this [53]. Bacteria survive in almost every aspect of nature that causes pathogenic, a virtue that is beneficial to humans and essential for the environment. Nearly 76 million ailments, 325000 hospitalizations, and 5000 deaths materialize in the United States each year due to food borne pathogens [54]. Contamination of bacteria from water supplies is a significant issue in developing countries and developed countries. The four bacterial pathogens, such as Salmonella species (spp.), Listeria monocytogenes, Campylobacter jejuni, and Escherichia coli (E. coli) O157:H7, accounted for roughly 67% of food-related deaths. To date, all these pathogens have been found in water supplies. Moreover, the main reservoir for entropathogenic E is known as several names of robust human hosts, i.e., Enteroinvasive (E. coli), strains of enterotoxigenic E. coli, and enterohemorrhagic E. coli. A novel MoS_2-based SPR sensor has been performed with numerical analysis for the identification of pseudomonas, such as bacteria by an SPR biosensor with very high efficiency. J. P. Nataro was utilized the three RI of bacteria concentration for tolerating the result with other structures, such as graphene-based and conventional SPR sensors [55].

The 17β- estradiol is one of the Endocrine-disrupting chemicals that is pretend as a significantly cruel due to the permissible estrogen effect. To preserve environmental and public health, the detection of these chemicals has been necessitated within the natural systems—different types of investigation instrumental techniques, such as gas chromatography, mass spectrometry, and high-performance liquid chromatography. These techniques are susceptible to these toxic chemicals, and very challenging to handle and commit a long period. This challenge has been leading many researchers to perform a more straightforward and effective biosensor system for chemical sensing. The human estrogen receptor has been ordinarily employing for 17-estradiol ascertainment in biosensor systems [56,57,58]. The detection process was performed at a linear dynamic range from 0.01 ng/mL-1000 ng/mL, with the lowest observable concentration at 10 pg/mL, and with shyness ranging from 85% to 15%. IC50signified the analyte absorption 1 ng/mL inducing 50% of the SPR signal inhibition. The proposed configuration of the immunosensor signifies extremely specific and selective for the estradiol [59]. Several harmful effects transpired due to human activity and industrial development, such as various potentially dangerous human-made by-products, chemicals produced in the combustion, and widespread in the environment. The principles of the SPR, test arrangement, surface amendment methods, and signal growth were presented as outlined of the paper. The SPR sensor utilization was also explored in the past decade in the identification of pesticides, polycyclic aromatic hydrocarbons, heavy metals, and polychlorinated biphenyls [60]. D. Michel had proposed the SPR experimental set up for detecting the Xanthan Gum employing the go Au as a metal film. The performance demonstrated the SPR sensor competently detecting the polysaccharide molecules, such as Xanthan gum up to 0.22 g/L. Moreover, the correlation between the reflected optical power and the dissolved Xanthan gum concentration is linear for the Concanavalin A, deposited on the metal film [61]. We have presented the different existing prism-based SPR structures for developing its performance and applications. This literature concluded the prism-based SPR sensor is a beneficial device for effective and label-free processing in a real-time biomolecule and biomedical field applications. The advancement of prism-based SPR sensors has been discussed in the next section.

3. Fiber optic based SPR sensor

The prism-based SPR operates with the TIR principle that ensues at the P-M interface when the incident angle is greater than the critical angle. Thenceforth, SPs excite at the surface, composing the EW on either side of the P-M medium. The same principle appears in the optical fiber-based SPR sensor except that the core-cladding interface is replaced instead of the P-M interface. Guided rays of the incident light pass through the core of the fiber. The EW propagates along with the core-cladding interface in the fiber case. The SPR sensor conforms the ATR principle to the Kretschmann's configuration for the detection mechanism. A fiber optic core–metal film–sensing medium forms the fiber-

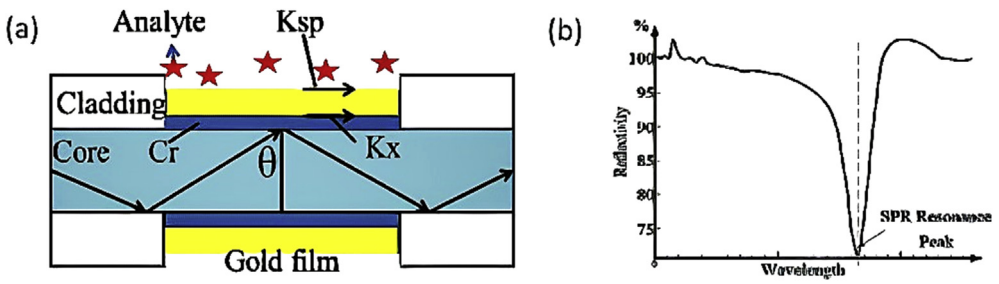

Figure 10. (a) The canonical structure of optical fiber-based SPR. (b) SPR resonance peak of optical fiber based SPR by employing wavelength interrogation.

based SPR sensor for the process is acknowledged, as presented in Fig. (10a). The middle portion of the cladding is extracted and coated around with the thin metal films (Au, Ag, Cu, or Al) with the thickness of d; Fig. (10b) presents the resonance peak of fiber based SPR sensor at resonance condition employing the wavelength interrogation. The polychromatic light source drives into one side of the fiber with decent optics and detects the transferred light at another end. J. Homola et al. reported the side polished SPR sensor with single-mode optical fiber, which has a thin metal covering layer, represented in Figure 11 [62]. Figure 12 served the probe fabrication by composing and surfacing the metallic films over the etched portion of the fiber core.

A circular-shaped high-birefringence (Hi-Bi) photonic crystal fiber-based SPR sensor was erected with Finite-difference Time-domain (FDTD), and TiO_2 materials. These properties were acquired by FEM (Finite Element Method), utilizing the COMSOL software. The results are displayed as follows: maximum wavelength-sensitivity (WS) 25000nm/RIU, Amplitude-sensitivity (AS) 1411 RIU^{-1} for RI 1.33–1.38 [63]. F. Wang et al. was proposed the SPR sensor with two parallel photonic crystal fibers (PCF) and a D-shaped structure. The Au was employed as a metal material. It used COMSOL software to analyze the performance parameters at the low RI at near-infrared (NIR) wavelength. The maximum spectral S of 13,500 nm/RIU, resolution of 7.41×10^{-6} RIU at RI range of 1.27–1.32 [64]. Z. Zhang et al. designed the SPR based on polymer tipped optical fiber (PTOF) with different metal materials, such as Au, Ag, Cu, Al, and TiO_2. Two various tools, such as the FDTD method and opti FDTD software, were utilized for the performance analysis at different analyte RIs. The results proved that S of 3798 nm/RIU at analyte RI of 1.333, 5708 nm/RIU at 1.383. Therefore, the authors concluded that Ag, Cu, act suitable metals for PTOF-based SPR because it renders high FOM, S, and minimum reflectivity [65].

N. Polley et al. was designed the optical fiber-based sensor's periodic hole array for signal transduction, using chemical wet lab techniques, convenient and low-cost methods. The sensor renders the massive throughput by adopting this approach and is ideal for commercialization, utilizing batch processing with S of (420 ±83) nm/RIU [66]. H. Qian et al. defined the convenient and low-cost principles for label-free bio-sensors, which are exhibited in [67] —externally sensitive protein detection in human serum samples with potential for further clinical diagnostics. Acetylcholine has been entrusted with behavioral conditions such as learning, memory, attention, excitement, and muscle contraction. Moreover, it plays an integral part in the functioning of the nervous system. K. Ravi et al. introduced the experimental operation on characterization and fabrication of fiber optic (FO)-SPR to the exposure of acetylcholine. This sensor designed by employing Ag, Ta2O5, which are significantly increasing the electrical field's intensity at the sensing surface. Consequently, an influential generation of SPR signal that enhances the S of the sensor [68]. V. Semwal et al. was designed the novel FO-SPR was designed by applying the Ag-rGO-pani as a metal film. Moreover, it utilized the X-ray diffraction, Fourier transforms infrared spectroscopy and Raman for acquires its characterization from the scanning and the transmission electron microscopy. The sensor has furnished the S of 75.09 nm/pH at the pH 11.35 due to the change in the rGO-Paninano-composite optical band-gap at small and high sample pH values (i.e., 2.4–11.35). Hence, the sensor unfolds several benefits, such

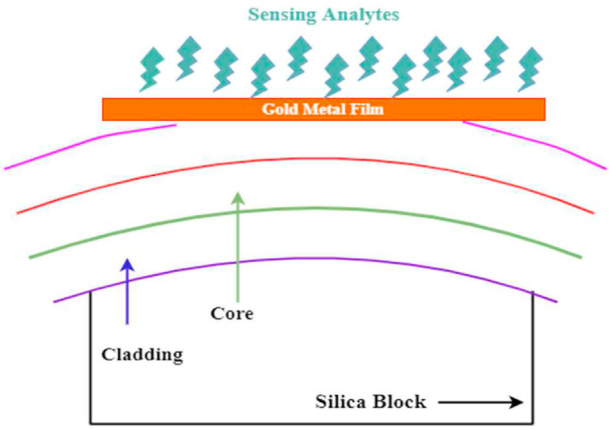

Figure 11. Side polished view of the Fiber-based SPR Sensor.

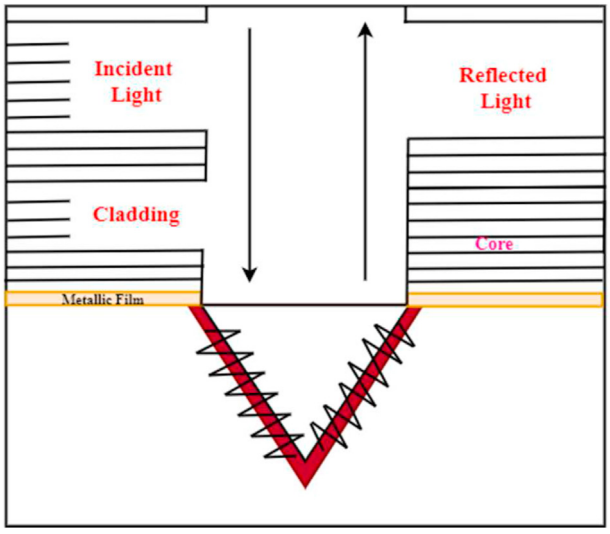

Figure 12. Fiber Optic-based SPR micro-sensor ([14], Figure 3).

as compact size, low cost, high S, reliability, repeatability, and remote sensing capability [69]. W. Qi et al. had fabricated a novel FO-SPR with Au-graphene-staphylococcal protein A and co-modified the tilted fiber Bragg grating. The proposed sensor was demonstrated a huge S in detecting human immunoglobulin G. The biosensor offers several advantages, such as rapid response, small size, high S, label-free, and manufacturing ease. It implements a new approach to detect the low amount of the great rendering potential, a biological solution for the biochemical field applications. The performance exhibited the S and limit of detection are 0.096 dB/g/mL and 0.5 g/mL, respectively [70]. F. Zha et al.was presented the PCF-SPR sensor with a D-shaped hole for utilizing in real-time diagnostic purposes, such as chemistry, biomedicine, advanced optics, and chemical detection. The sensor can minimize the coupling effect and capable sensing infiltration. The sensor had enhanced the WS's performance of 14,600 nm/RIU, and AS of 1475 RIU^{-1}, FOM of 618 for RI varied from 1.30 to 1.42. Therefore, this sensor contributes to detecting a wide range of capabilities and broad application prospects in biomedical fields [71]. Furthermore, a novel Smartphone-based sensor has been proposed by Q. Liu et al., consisting of the red-green dual color with diffraction gratings narrow-band filters to accomplish the high S, spectral data, and less false detections. The S development of SPR performance in an aqueous environment by employing the Ag/Au bi-layer structure at the central precinct of visible spectrum. The authors have performed this experimentally, and the consequence was that the quadratic outcome in the RI range is 1.325–1.344 ($R^2 = 0.992$). The maximum noteworthy S of 18.59/RIU and a resolution of 5.3×10^{-4} RIU at the RI of linear outcome range of 1.325–1.330 [72]. This new structure confirmed an exceptional potential as the point-of-need and point-of-care platform for the food protection, healthcare, and erudition of the environment, particularly in rural and remote areas. H. Fu et al. was demonstrated theoretical analysis of graphene-based FO-SPR and it furnished excellent S performance than the conventional sensor. Theoretically, the sensor's S was amplified by 50% with 20 graphene layers [73]. Z. Fan et al. had proposed the Au coated PCF-SPR sensor for S analysis by considering FEM software. The performance demonstrated the S is directly proportional to the RI analysis. For phase-matching conditions, three types of SPP modes and the primary modes are formed in the PCF-SPR. These modes exhibit because the photon and electron resonance rise simultaneously as the RI analyte increases. The dispersion similarities of two lowest-order SP modes have emerged for a structure comprising a thin silver sheet around a diminished fiber cladding; the Mode splitting is created by decreasing metal thickness. The phase-matching condition's fulfillment was tested, adopting an inventory of the SPs and fiber modes [74]. N. Cennamo et al. also presented the low-cost computational and experimental reports for the SPR configuration. The sensor relayed on the plasmonic sensor platform and active higher-order filtering modes in the multimode plastic fiber—moreover, the sensor utilizing a tapered optical plastic fiber at the sensor network [76]. A RI and temperature sensor structure is based on hybrid mechanisms in a D-shaped all-solid photonic crystal fiber proposed in [77]. L. Peng was introduced an innovative FO-SPR sensor with ring core microstructure and Ag metal film [78]. M. Li et al. had developed the PCF filter that offers excellent benefits, such as narrow width and single polarization. This advantages are transpired through a complete modal vector solver, relying on SPR theory at the FEM [79]. L. C. C. Coelho et al. suggested the multiplexing the FO-SPR sensor stationed in the ladder topology, appraising the intensity analysis, and inscribed in wavelength with consolidating individual sensor with various FBGs. The highest S of 5000 nm/RIU and RI resolution in the order of 10^{-4} RIU [80]. N.luan et al. was proposed the exposed-core micro-structured optical fiber-SPR sensor, which was mounted with a silver cable in the [81]. A hollow fiber-based SPR sensor has intended the realization of fast analyte RI detection [82]. In [83], N. Jing et al. was introduced an SPR effect-based RI sensor. Moreover, S.K. Mishra was developed a commercial POF with a D-shaped macro-bend structure using heat setting and side polishing techniques to expose the core and enhance S for the RI. The authors in [84] manufactured and characterized the profoundly sensitive FO-SPR sensor at low concentrations for ammonia gas detection. This literature confirmed that the FO-SPR sensors are advanced technology of conventional SPR sensors. Moreover, researchers proposed several FO-SPR biosensors for different applications, which can benefit society and sustain human healthy by detecting several diseases.

4. Waveguide based SPR sensor

For further advancement of the biosensor field, many researchers have proposed the waveguide based SPR sensors. The Planar optical waveguides (POW) manifest a great promise in the realization of novel chemical and biochemical sensors. This sensor utilizes evanescent fields to analyze specially sensitized films on the waveguide surface. The potential advantages of waveguide-coupled systems are that efficiently coupling with optical fibers for instrumentation communication. The single optical 'chip' integrates with the multiple sensors by applying manufacturing technologies from microelectronics. Several waveguide-based systems were implemented the biosensors to miniaturize the SPR [85,86]. Figure (13a) presented the canonical representation of a waveguide SPR sensor, consolidate a buffer layer. The incident light passes towards the waveguide core and then searches for the environment's variations by employing a directed and plasmonic mode coupling. The phase-matching action must be satisfied between the waveguide and plasmon modes to trigger the SPs effectively. Figure (13b) represented numerous precincts of the sensor and the relevant field portraits. Generally, one should employ a single-phase waveguide to plasmon's resonant excitation with all power moving in a single core Gaussian. Most incident light energy is conveyed as plasmon mode at the end of the waveguide core. J. S. Wilkinson utilized a comparative approach to incorporate various compact structures of the SPR biosensors based on planar waveguides [85]. Nevertheless, the SPR coupling has been delivered for these single-mode, low index contrast waveguides at primarily grazing modal incidence angles on the metal sheet. Coupling at these grazing incidence angles results, from the SPR theory, in an eventual decrease in S.

Furthermore, Figure 14 depicts the waveguide structure with a leaky mode-dependent device termed a resonance waveguide grating biosensor. Two-dimensional (2D) gratings have covered the gap amidst gratings and introduced among the cover and substrate layers. The waveguide was created in gratings when the active grating index's refraction is far higher than the substrate. Narrowband wavelengths propagate through the waveguide, coupled it from either side of the grating, and reflected towards the detector [86]. Reflected wavelength varies according to the changes in the sensing layer [86,87]. Corning Inc. introduced its Epic version, and for the enhancement of S, both companies have provided 96-, 384-, and 1536-well plates, which is more suitable for delivering huge throughput selection [88,89].

The authors need to perform the theoretical analysis with Resonance Waveguide Grating (RWG) to optimize the grating structure's design and fabrication [89]. We need to accept the RWG biosensors and SPR and RM to determine the small molecules' proteins [91,92,93]. In cell development and migration, cell adhesion changes and extracellular changes were acts a key role. It proved that a variety of diseases also lead to specific changes in cell adhesion [90]. A new optical inter-connect chip (OIC) subsisted of a photonic crystal SPR as a biosensor, a Fabry-Perot (FP) laser as a light source, and a photodetector. The responsivity and performance of OIC were observed corresponding to the various urea molarities. To examine the development of the OIC ingests through simulation utilizing the Lumerical interconnect solver. The laser emits a wavelength of 800 nm, and the threshold current noted 0.015A at the output power of 0.0021W, while the PD at 1.0 A/W sensitive. Increasing the RI value is 1.333–1.335 raises the responsivity of OIC at granted optical energy of 0.025 μW from 0.4 A/W to 0.8 A/W. This OIC model operates ideal in medical applications for biosensor chips for disease detection due to RI changes [93]. It is most outstandingly used to monitor

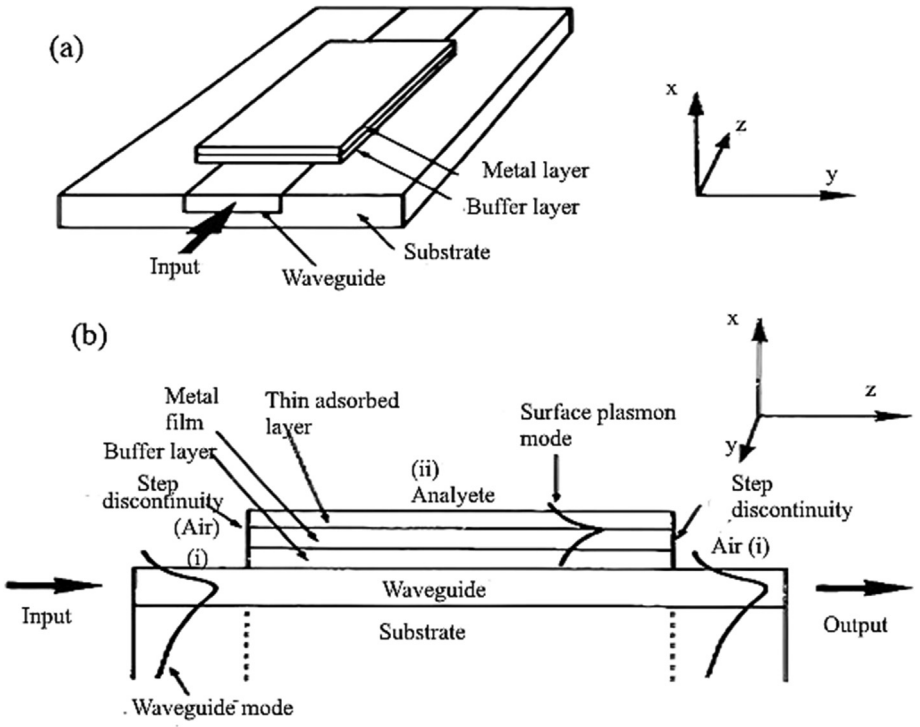

Figure 13. (a) Schematic representation of a waveguide SPR sensor incorporating a buffer layer. (b) The below picture depicts the several precincts of the sensor and the relevant field portraits (This figure copied from the Elsevier, Type of use: Reuse in journal/magazine, License number: 4892281394552, License date: 19/08/2020, licensed content publisher: Elsevier, Ref. [85], Figure 1).

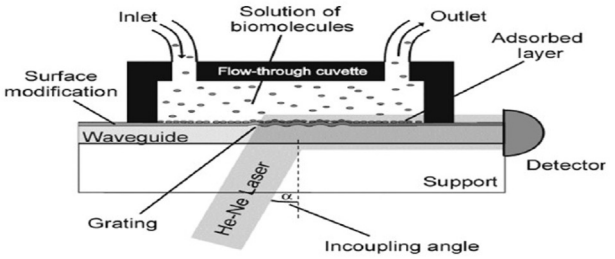

Figure 14. Resonance Waveguide grating SPR structure.

the protein mass redistribution and live cell's organelles ahead dealing with test agents [89,94,95,96]. These changes make in the real-time that it a gorgeous makes this an essential method for drug discovery. Evaluating cells was of drawback with this biosensor because of the enormous size of cells, and the penetration depth of an EW was limited (~100 nm). This effect leads to misleading as annotations are made only to a partial part of the cell [95].

An angular interrogation-based SOI (Si-on-Insulator) waveguide SPR sensor is designed, and the metal film thickness is optimized to acquire enhanced performance parameters. The curve dip can be achieving much sharper than the silica prism-based SPR sensors due to Si's high RI. Hence, dip variation can be more easily differentiated [97]. A high-performance bimetallic-based SPR sensor was performed on periodic multilayer waveguide and SPR active metals, such as Au and Al. The S and D.A. for bimetallic (Au + Al) configuration attainable adequately tailored in terms of S (5340 nm-RIU^{-1}) and equal D.A. ($\sim 130\ \mu m^{-1}$) by employing pair-mode theory. The geometry's impressive majority characteristic suggested this design's feasibility in any desired spectral region [98]. Glycan-based detection helps differentiate within H3N2 and H5N1 viruses, utilizing the application of the waveguide sensor system. Moreover, this topic concerns the waveguide-mode sensor immunosorbent assay and SPR [99].

The Gaussian-like leaky core mode of metal-covered 1D photonic crystal waveguide can attest resonant excitation of a plasmon. Sensing applications and significant advantages over existing waveguide-based schemes have been discussed [100]. A graphic novel RI sensor based on two metal-insulator-metal asymmetric couplings waveguides were proposed with a ring resonator and investigated [101]. S. K. Mishra et al. had proposed a RI sensor in a polymer channel waveguide coated with a Cu film based on the SPR concept. For fabrication, they have utilized the 40 nm Cu film covered with 10 nm Ag. The authors analyzed this sensor performance was through theoretical and experimental analysis. Moreover, the results were showed in [101] that approximately equal as demonstrated in [102]. In [103], N. Rezae et al. has suggested that using a bimetallic structure for a D-shaped optical fiber SPR based on waveguide coupled mode. The Finite-Time Domain Difference approach was applied to analyze the proposed construction and boost its flexibility. Maximum S leads to about 6140.2 nm/RIU. Finally, R. Komai et al. was designed a waveguide-based SPR sensor, which has been equipped with a single waveguide for double analyte detections, and ammonia and water vapor sensing [104]. Here, the authors have been proposed several structures for developing the waveguide-based SPR sensor. Therefore, waveguide-based SPR sensors are potent devices in the field of biosensors in order to enhance the performance of the sensor, and it opens new platforms in the biomolecules and biosensing applications.

5. Future scope

For decades, the number of diseases in human beings have been regularly increasing. We must develop sensing devices that can easily sense and easily be accessible. From the user aspect, this information can be purchased from the independent equipment, positive or negative examination syndrome, or the contaminant's existence in a sample interest. This information resides in a double problem for developers and

researchers. On the one hand, any application of biosensors relies upon the viability of the biomarkers or analytes detected to yield specific syndrome. The comprehensive list of biomarkers correlating with multiple cancers and dangerous diseases that can proposes the potential advantage of robust biosensor technology, but it exhibits significant challenges. In many situations, the analytes of interest are presenting in a complex medium at low concentration. Therefore, one of the challenges are the identification of multiple analytes required for accurate diagnosis rendered the genetic or host response differences.

The second challenge is that endures in the instrumentation, and the center is on affording relatively low-cost, robust multiple analyte detection biosensor platforms. The existed work has been operating on visible range wavelength for the only S improvement of the prism-based SPR sensor with few applications by employing MATLAB tool. Hence, the third challenge is that the new authors need to develop the novel structures, enhancing all performance parameters, such as S, D.A., Q.F., and FOM for different applications. Moreover, researchers need to establish the prism-based SPR for more significant sensing parameters at near-Infrared and non-visible ranges by numerical methods.

Furthermore, the fourth challenge is that researchers necessitate developing more applications by SPR sensors for society's benefit because nowadays, diseases have been increasing a lot. Also, enhancing the performances of fiber-based SPR and waveguide-based SPR at the high-frequency range for different applications can be considered as the fifth challenge. One more significant challenge for new researchers in the biosensor field is the lack of experimental work development. In addition, the SPR based sensors beget vast open research in several areas. Biosensors, nano-sensors, and photonic crystal-assisted sensors are primarily bound to come across more advances in the expectations. The other challenge is the fabrication of non-specific interactions with unwanted molecules amid the sensor's surface and the RI background mutations. Those variations can be due to fluctuations in temperature, moisture, and composition. The consumer demands the above mentioned parameters to drive as the future scope of the SPR based biosensors. Therefore, the sensor must be presented to more consumers graciously. The challenges helped to the new researchers for developing the biosensors in this field.

6. Conclusion

The comprehensive review of SPR based biosensors, such as prism-based SPR, fiber-based SPR, waveguide-based SPR sensors and their applications, have been presented in this paper. The Au-BP structure of prism-based SPR sensors demonstrated improved S, and the Ag-Si-BP design furnished the enhanced parameters in terms of D.A., Q.F., and FOM. Therefore, BP is highly recommended as a dielectric material in order to improve the performance of prism-based SPR sensors due to the unique properties, such as high absorption energy and efficient biomolecule bonding. It was found in the literature that PTOF-based FO-SPR sensors using FDTD software demonstrated substantial enhancement of S and FOM. Also, the existing work based on the FO-SPR sensors has been studied by considering COMSOL software with different types of structures. Furthermore, the bi-metallic Au, Al waveguide structures were shown high D.A and S. In order to increase sensitivity, a D-shaped FO-SPR based waveguide structure has been used in the literature. In addition, the chronologically cumulative and systematic evolution of the recorded SPR based sensors over the past few years are explained in detail. This paper can be definitely motivated the researchers for future research and development in the field of SPR based sensors.

Declarations

Author contribution statement

All authors listed have significantly contributed to the development and the writing of this article.

Funding statement

This research did not receive any specific grant from funding agencies in the public, commercial, or not-for-profit sectors.

Data availability statement

No data was used for the research described in the article.

Declaration of interests statement

The authors declare no conflict of interest.

Additional information

No additional information is available for this paper.

References

[1] B. Liedberg, C. Nylander, I. Lunstrom, Surface plasmon resonance for gas detection and biosensing, Sens. Actuators, B 4 (1983) 299–304.
[2] R.W. Wood, On a remarkable case of uneven distribution of light in a diffraction grating spectrum, Phys. Soc. 18 (1) (1902) 269.
[3] J. Zenneck, Uber die FortpflanzungebenerelektromagnetischerWellenlangseinerebenenLeiterflache und ihreBeziehungzurdrahtlosenTelegraphie, Ann. Phys. 328 (10) (1907) 846–866.
[4] A. Sommerfeld, Propagation of waves in wireless telegraphy, Ann. Phys. 28 (1909) 665–736.
[5] R.H. Ritchie, Plasma losses by fast electrons in thin films, Phys. Rev. 106 (1957) 874–881.
[6] C.J. Powell, J.B. Swan, Effect of oxidation on the characteristic loss spectra of aluminum and magnesium, Phys. Rev. 118 (1960) 640–643.
[7] E.A. Stern, R.A. Ferrell, Surface plasma oscillations of a degenerate electron gas, Phys. Rev. 120 (1960) 130–136.
[8] A. Otto, Excitation of nonradiative surface plasma waves in silver by the method of frustrated total reflection, Z. Phys. 216 (4) (1968) 398–410.
[9] E. Kretschmann, H. Reather, Radiative decay of non-radiative surface plasmons excited by light, Zeit.Natur. 23 (12) (1968) 2135–2136.
[10] X.D. Hoa, A.G. Kirk, M. Tabrizian, Towards integrated and sensitive surface plasmon resonance biosensors: a review of recent progress, Biosens. Bioelectron. 23 (2) (2007) 151–160.
[11] J. Homola, S.S. Yee, G. Gauglitz, Surface plasmon resonance sensors: Review, Sens. Actuators, B 54 (1-2) (1999) 3–15.
[12] R. Ince, R. Narayanaswamy, Analysis of the performance of interferometry, surface plasmon resonance, and luminescence as biosensors and chemosensors, Analy.Chim. Acta 569 (1-2) (2006) 1–20.
[13] O.S. Wolfbeis, Fiber-optic chemical sensors and biosensors, Anal. Chem. 78 (12) (2006) 3859–3873.
[14] A.K. Sharma, R. Jha, B.D. Gupta, Fiber-optic sensors based on surface plasmonresonance: a comprehensive review, J. IEEE Sens. 7 (8) (2007) 1118–1129.
[15] R.H. Ritchie, Plasma losses by fast electrons in thin films, Phys. Rev. 106 (5) (1957) 874–881.
[16] C.J. Powell, J.B. Swan, Effect of oxidation on the characteristic loss spectra of aluminum and magnesium, Phys. Rev. 118 (3) (1960) 640–643.
[17] A. Otto, Excitation of nonradiative surface plasma waves in silver by the method of frustrated total refection, Z. Phys. 216 (4) (1968) 398–410.
[18] Y.K. Prajapati, A. Yadav, A. Verma, V. Singh, Effect of metamaterial layer on optical surface plasmon resonance sensor, J. Light Elec. Opt. 124 (18) (2013) 3607–3610.
[19] S. Pal, Y.K. Prajapati, J.P. Saini, V. Singh, Resolution enhancement of optical surface plasmon resonance sensor using metamaterial, Photonic Sens 5 (4) (2015) 330–338.
[20] J.B. Maurya, Y.K. Prajapati, A comparative study of different metal and prism in the surface plasmon resonance biosensor having MoS_2-graphene, Opt. Quant. Electron. 48 (5) (2016) 280.
[21] S. Pal, A. Varma, Y.K. Prajapati, J.P. Saini, Influence of black phosphorous on performance of surface plasmon resonance biosensor, Opt. Quant. Electron. 49 (12) (2017) 403.
[22] M.S. Rahman, M.S. Anower, M.R. Hasan, M.B. Hossain, M.I. Haque, Design and numerical analysis of highly sensitive Au-MoS_2-graphene based hybrid surface plasmon resonance biosensor, Optic Commun. 396 (2017) 36–43.
[23] J.B. Maurya, Y.K. Prajapati, V. Singh, J.P. Saini, R. Tripathi, Improved performance of the surface plasmon resonance biosensor based on graphene or MoS_2 using silicon, Optic Commun. 359 (2016) 426–434.
[24] J.B. Maurya, Y.K. Prajapati, V. Singh, J.P. Saini, R. Tripathi, Performance of graphene–MoS 2 based surface plasmon resonance sensor using silicon layer, Opt. Quant. Electron. 47 (11) (2015) 3599–3611.

[25] J.B. Maurya, Y.K. Prajapati, Influence of dielectric coating on performance of surface plasmon resonance sensor, Plasmonics 12 (4) (2017) 1121–1130.
[26] S. Pal, Y.K. Prajapati, J.P. Saini, V. Singh, Sensitivity enhancement of metamaterial-based surface plasmon resonance biosensor for near infrared, Opt. Appl. 46 (1) (2016).
[27] M.B. Hossain, M. Hassan, L.F. Abdulrazak, M.M. Rana, M.M. Islam, M.S. Rahman, Graphene-MoS_2-Au-TiO_2-SiO_2 hybrid SPR biosensor for formalin detection: numerical analysis and development, Adv. Mater. Lett. 10 (9) (2019) 656–662.
[28] Y. Xiang, J. Zhu, L. Wu, Q. You, B. Ruan, X. Dai, Highly sensitive terahertz gas sensor based on surface plasmon resonance with graphene, J. IEEE Photonics 10 (1) (2017) 1–7.
[29] L. Oliveira, A. Herbster, C. da Silva Moreira, F.H. Neff, A.M.N. Lima, Surface plasmon resonance sensing characteristics of thin aluminum films in aqueous solution, J. IEEE Sensors 17 (19) (2017) 6258–6267.
[30] Sinan Aksimsek, Zhipei Sun, Graphene-MoS_2heterostructure Based Surface Plasmon Resonance Biosensor, EMTS IEEE, 2016.
[31] J.N. Nur, F. Asrafy, K.N. Shushama, Highly Sensitive Surface Plasmon Resonance Biosensor Using WSe_2 and Silicon, iCEEiCT IEEE, 2018.
[32] M.M. Bari, A.K. Sarkar, S. Hossain, Sensitivity Analysis of a Graphene Based Surface Plasmon Resonance Biosensor in Terms of Number of Graphene Layers, ICECTE IEEE, 2016.
[33] H. Vahed, C. Nadri, Sensitivity enhancement of SPR optical biosensor based on Graphene-MoS_2 structure with nanocomposite layer, Opt. Mater. 88 (2019) 161–166.
[34] M.S. Islam, A.Z. Kouzani, E.D. Coyle, Theoretical Analysis of the Propagation of Surface Plasmon Waves in Multilayer Surface Plasmon Resonance Biosensor, PIERS IEEE, 2017.
[35] S. Pal, A. Verma, J.P. Saini, Y.K. Prajapati, Sensitivity enhancement using silicon-black phosphorus-TDMC coated surface plasmon resonance biosensor, IET Optoelectron. 13 (4) (2019) 196–201.
[36] R. Boruah, D. Mohanta, A. Choudhury, P. Nath, G.A. Ahmed, Surface plasmon resonance-based protein bio-sensing using a Kretschmann configured double prism arrangement, J. IEEE Sensors 15 (12) (2015) 6791–6796.
[37] G. Lan, Y. Gao, Surface plasmon resonance sensor with high sensitivity and wide dynamic range, IEEE Sens 18 (13) (2018) 5329–5333.
[38] A.A. Michelson, F.G. Pease, F. Pearson, Repetition of the michelson-morley experiment, JOSA 18 (3) (1929) 181–182.
[39] S.K. Raghuwanshi, M. Kumar, Highly dispersion tailored property of novel class of multimode surface plasmon resonance biosensor assisted by teflon and metamaterial layers, IEEE Trans. Instr. Meas. (2018).
[40] C.A. De Souza Filho, A.M. Lima, F.H. Neff, Modeling and temperature drift compensation method for surface plasmon resonance-based sensors, IEEE Sens 17 (19) (2017) 6246–6257 (2017).
[41] S. Scarano, S. Mariani, M. Minunni, SPR-based affinity biosensors as innovative analytical devices, J. LightwaveTechn. 33 (16) (2015) 3374–3384.
[42] V.M. Faca, K.S. Song, H. Wang, Q. Zhang, A.L. Krasnoselsky, L.F. Newcomb, R.R. Plentz, S. Gurumurthy, M.S. Redston, S.J. Pitteri, S.R. Pereira-Faca, A mouse to human search for plasma proteome changes associated with pancreatic tumor development, PLoS Med. 5 (6) (2008).
[43] S. Pal, A. Verma, S. Raikwar, Y.K. Prajapati, J.P. Saini, Detection of DNA hybridization using graphene-coated black phosphorus surface plasmon resonance sensor, Appl. Phys. A 124 (5) (2018) 394.
[44] M.S. Rahman, M.R. Hasan, K.A. Rikta, M.S. Anower, A novel graphene coated surface plasmon resonance biosensor with tungsten disulfide (WS_2) for sensing DNA hybridization, Opt. Mater. 75 (2018) 567–573.
[45] B. Meshginqalam, J. Barvestani, Performance enhancement of SPR biosensor based on phosphorene and transition metal dichalcogenides for sensing DNA hybridization, IEEE Sens 18 (18) (2018) 7537–7543.
[46] Y. Vasimalla, H. Pradhan, R. Pandya, SPR performance enhancement for DNA hybridization employing Black Phosporous, Silver and Silicon, Appl. Optic. 59 (24) (2020) 7299–7307.
[47] S. Ahmed, S. Kabir, Copper-Germanium-Graphene Based Highly Sensitive Plasmonic Biosensor for Protein Detection, IC4ME2 IEEE, 2018.
[48] W. Wu, A. Katsnelson, O.G. Memis, H. Mohseni, A deep sub-wavelength process for the formation of highly uniform arrays of nanoholes and nanopillars, Nanotechnology 18 (48) (2007) 485302.
[49] F. Said, P.S. Menon, M.N. Nawi, A.R. Zain, A. Jalar, B.Y. Majlis, Copper-Graphene SPR-Based Biosensor for Urea Detection, ICSE IEEE, 2016.
[50] N.A. Jamil, P.S. Menon, F.A. Said, K.A. Tarumaraja, G.S. Mei, B.Y. Majlis, Graphene-Based Surface Plasmon Resonance Urea Biosensor using Kretschmann Configuration, RSM IEEE, 2017.
[51] N.A. Jamil, N.B. Khairulazdan, P.S. Menon, A.R. Zain, A.A. Hamzah, B.Y. Majlis, Graphene-MoS2 SPR-Based Biosensor for Urea detection, ISESD IEEE, 2018.
[52] N.A. Jamil, P.S. Menon, G.S. Mei, S. Shaari, B.Y. Majlis, Urea Biosensor Utilizing Graphene-MoS_2 and Kretschmann-Based SPR, IEEE, 2017.
[53] P.S. Mead, L. Slutsker, V. Dietz, L.F. McCaig, J.S. Bresee, C. Shapiro, P.M. Griffin, R.V. Tauxe, Food-related illness and death in the United States, Emerg. Infect. Dis. 5 (5) (1999) 607.
[54] J.B. Maurya, Y.K. Prajapati, R. Tripathi, Effect of molybdenum disulfide layer on surface plasmon resonance biosensor for the detection of bacteria, Siliconindia 10 (2) (2018) 245–256.
[55] J.P. Nataro, J.B. Kaper, Diarrheageniceschericia coli, Clin. Microbiol. Rev. 11 (1) (1998) 142–201.
[56] S. Kumbhat, R. Gehlot, K. Sharma, U. Singh, V. Joshi, Surface plasmon resonance based indirect immunoassay for detection of 17β-estradiol, J. Pharmaceut. Biomed. Anal. 163 (2019) 211–216.
[57] J.K. Seifert, D.L. Morris, World survey on the complications of hepatic and prostate cryotherapy, J. Surg. 23 (2) (1999) 109–114.
[58] H.D. Butala, A. Ramakrishnan, A. Sadana, A mathematical analysis using fractals for binding interactions of estrogen receptors to different ligands on biosensor surfaces, Sensor. Actuator. B Chem. 88 (3) (2003) 266–280.
[59] E. Wozei, S.W. Hermanowicz, H.N. Holman, Developing a biosensor for estrogens in water samples: study of the real-time response of live cells of the estrogen-sensitive yeast strain RMY/ER-ERE using fluorescence microscopy, Biosens. Bioelectron. 21 (8) (2006) 1654–1658.
[60] M. Mahmoudpour, J.E. Dolatabadi, M. Torbati, A. Homayouni-Rad, Nanomaterials based surface plasmon resonance signal enhancement for detection of environmental pollution, Biosens. Bioelectron. 127 (2019) 72–84.
[61] D. Michel, F. Xiao, L. Skillman, K. Alameh, Surface plasmon resonance sensor for in situ detection of xanthan gum, J. IEEE Quant. Elect. 22 (3) (2015) 379–382.
[62] J. Homola, R. Slavik, Fibre-optic sensor based on surface plasmon resonance, Electron. Lett. 32 (5) (1996) 480.
[63] M.S. Islam, C.M. Cordeiro, J. Sultana, R.A. Aoni, S. Feng, R. Ahmed, M. Dorraki, A. Dinovitser, B.W. Ng, D. Abbott, A hi-Bi ultra-sensitive surface plasmon resonance fiber sensor, IEEE Access 7 (2019) 79085–79094.
[64] F. Wang, C. Liu, Z. Sun, T. Sun, B. Liu, P.K. Chu, A highly sensitive SPR sensors based on two parallel PCFs for low refractive index detection, IEEE Photonics 10 (4) (2018) 1–10.
[65] Z. Zhang, F. Chu, Z. Guo, J. Fan, G. Li, W. Cheng, Design and optimization of surface plasmon resonance sensor based on polymer-tipped optical fiber, J. LightwaveTechn. 37 (11) (2019) 2820–2827.
[66] N. Polley, S. Basak, R. Hass, C. Pacholski, Fiber optic plasmonic sensors: providing sensitive biosensor platforms with minimal lab equipment, Biosens. Bioelectron. 132 (2019) 368–374.
[67] H. Qian, Y. Huang, X. Duan, X. Wei, Y. Fan, D. Gan, S. Yue, W. Cheng, T. Chen, Fiber optic surface plasmon resonance biosensor for detection of PDGF-BB in serum based on self-assembled aptamer and antifouling peptide monolayer, Biosens. Bioelectron. 140 (2019) 111350.
[68] K. Ravi, B.D. Gupta, Fiber-optic SPR based acetylcholine biosensor using enzyme functionalized Ta_2O_5Nanoflakes for alzheimer's disease diagnosis, J. LightwaveTechn. 36 (18) (2018) 4018–4024.
[69] V. Semwal, B.D. Gupta, Highly sensitive surface plasmon resonance based fiber optic pH sensor utilizing rGO-Pani nanocomposite prepared by in situ method, Sensor. Actuator. B Chem. 283 (2019) 632–642.
[70] W. Qi, J.Y. Jing, B.T. Wang, Highly sensitive SPR biosensor based on graphene oxide and staphylococcal protein A Co-modified TFBG for human IgG detection, IEEE Transactions Inst. Meas. (2018).
[71] F. Zha, J. Li, P. Sun, H. Ma, Highly sensitive selectively coated D-shape photonic crystal fibers for surface plasmon resonance sensing, Phys. Lett. 383 (15) (2019) 1825–1830.
[72] Q. Liu, Y. Liu, H. Yuan, F. Wang, W. Peng, A smartphone-based red-green dual color fiber optic surface plasmon resonance sensor, IEEE Photon. Technol. Lett. 30 (10) (2018) 927–930.
[73] H. Fu, S. Zhang, H. Chen, J. Weng, Graphene enhances the sensitivity of fiber-optic surface plasmon resonance biosensor, J. IEEE Sens. 15 (10) (2015) 5478–5482.
[74] Z. Fan, Surface plasmon resonance refractive index sensor based on photonic crystal fiber covering nano-ring gold film, Opt. Fiber Technol. 50 (2019) 194–199.
[76] N. Cennamo, L. Coelho, D.F. Santos, J.M. Baptista, A. Guerreiro, P.A. Jorge, Modal filtering for optimized surface plasmon resonance sensing in multimode plastic optical fibers, IEEE Sens 15 (11) (2015) 6306–6312.
[77] N. Luan, J. Yao, Refractive index and temperature sensing based on surface plasmon resonance and directional resonance coupling in a PCF, IEEE Photonics 9 (2) (2017) 1–7.
[78] L. Peng, G. Zhou, M. Li, Z. Hou, C. Xia, S. Ge, Surface plasmon resonance sensor based onMicrostructured optical fiber with ring-core configuration, IEEE Photonics 8 (5) (2016) 1–11.
[79] M. Li, L. Peng, G. Zhou, B. Li, Z. Hou, C. Xia, Design of photonic crystal fiber filter with narrow width and single-polarization based on surface plasmon resonance, IEEE Photonics 9 (3) (2017) 1–8.
[80] L.C.C. Coelho, J.M.M.M. de Almeida, H. Moayyed, J.L. Santos, D. Viegas, Multiplexing of surface plasmon resonance sensing devices on etched single-mode fiber, J. LightwaveTechn. 3 (2) (2015) 432–438.
[81] N. Luan, J. Yao, Surface plasmon resonance sensor based on exposed-core microstructured optical fiber placed with A silver wire, IEEE Photonics 8 (1) (2016) 1–8.
[82] N. Luan, J. Yao, High refractive index surface plasmon resonance sensor based on a silver wire filled hollow fiber, IEEE Photonics 8 (1) (2016) 1–9.
[83] N. Jing, J. Zhou, K. Li, Z. Wang, J. Zheng, P. Xue, Refractive index sensing based on a side-polished macrobend plastic optical fiber combining surface plasmon resonance and macrobending loss, IEEE Sens 19 (14) (2019) 5665–5669.
[84] S.K. Mishra, S. Bhardwaj, B.D. Gupta, Surface plasmon resonance-based fiber optic sensor for the detection of low concentrations of ammonia gas, IEEE Sens 15 (2) (2015) 1235–1239.
[85] R.D. Harris, J.S. Wilkinson, Waveguide surface plasmon resonance sensors, Sensor. Actuator. B Chem. 29 (1-3) (1995) 261–267.
[86] B.D. Gupta, A.K. Sharma, Sensitivity evaluation of a multi-layered surface plasmon resonance-based fiber optic sensor: a theoretical study, Sensor. Actuator. B Chem.

107 (1) (2005) 40–46.
[87] B.T. Cunningham, Label-free assays on the BIND system, J. Biomol. Screen 9 (6) (2004) 481–490.
[88] Y. Fang, Non-invasive optical biosensor for probing cell signaling, Sensors 7 (10) (2007) 2316–2329.
[89] Y. Fang, Resonant waveguide grating biosensor for microarrays, Opt. Guided-wave Chem. Biosens. 8 (1) (2010) 27–42.
[90] J. Yih, Y.M. Chu, Y.C. Mao, W.H. Wang, F.C. Chien, C.Y. Lin, K.L. Lee, P.K. Wei, S.J. Chen, Optical waveguide biosensors constructed with subwavelength gratings, Appl. Optic. 45 (9) (2006) 1938–1942.
[91] Y. Fang, Label-free and non-invasive biosensor cellular assays for cell adhesion, J. Adhes. Sci. Technol. 24 (5) (2010) 1011–1021.
[92] J.T. Parsons, A.R. Horwitz, M.A. Schwartz, Cell adhesion: integrating cytoskeletal dynamics and cellular tension, Nat. Rev. Molec. Biol. 11 (9) (2010) 633–643.
[93] K.A. Tarumaraja, P.S. Menon, F.A. Said, N.A. Jamil, G.S. Shaari, B.Y. Majlis, Optical interconnect chip with SPR-based photonic crystal waveguide sensor, TENCON IEEE Reg (2017).
[94] Y. Fang, A.M. Ferrie, N.H. Fontaine, J. Mauro, J. Balakrishnan, Resonant waveguide grating biosensor for living cell sensing, Biop 91 (5) (2006) 1925–1940.
[95] B. Xi, N. Yu, X. Wang, X. Xu, Y. Abassi, The application of cell-based label-free technology in drug discovery, Biotechnology 3 (4) (2008) 484–495.
[96] Y. Fang, Label-free optical biosensor for ligand-directed functional selectivity acting on β2 adrenoceptorin living cells, FEBS Lett. 582 (5) (2008) 558–564.
[97] S. Fan, Mingyu Li, Jian-Jun He, Investigation of a SPR Waveguide Sensor Based on Angular Interrogation, ACPCE IEEE, 2010.
[98] T. Srivastava, R. Jha, R. Das, High-performance bimetallic SPR sensor based on periodic-multilayer-waveguides, IEEE Photon. Technol. Lett. 23 (20) (2011) 1448–1450.
[99] K. Awazu, M. Fujimaki, S.C. Gopinath, Palmtop waveguide-mode sensor: comparison of sensitivity and subtyping of influenza viruses with SPR, ELISA and Immunochromatography, IEEE Sens (2013) 1–3.
[100] M. Skorobogatiy, A.V. Kabashin, Photon Crystal Waveguide-Based Surface Plasmon Resonance Biosensor, CLEO Baltimore, 2007, pp. 1–2.
[101] S. Zou, F. Wang, R. Liang, L. Xiao, M. Hu, A nanoscale refractive index sensor based on asymmetric plasmonic waveguide with a ring resonator: a review, Sensors 15 (2) (2015) 646–650.
[102] S.K. Mishra, B. Zou, K.S. Chiang, Surface-plasmon-resonance refractive-index sensor with Cu-coated polymer waveguide, IEEE Photon. Technol. Lett. 28 (17) (2016) 1835–1838.
[103] N. Rezaei, A. Yahaghi, A high sensitivity surface plasmon resonance D-shaped fiber sensor based on a waveguide-coupled bimetallic structure: modeling and optimization, IEEE Sens 14 (10) (2014) 3611–3615.
[104] R. Komai, H. Honda, A. Baba, K. Shinbo, K. Kato, F. Kaneko, Simultaneous detection of ammonia and water vapors using surface plasmon resonance waveguide sensor, ISEIM (2014) 284–286.